BIOCELL

Tech Science Press

http://doi.org/10.32604/biocell.2026.077413

ARTICLE

Overexpression of GluN2B Regulates Neuroinflammation through the BDNF/TrkB Signaling Pathway to Improve Postoperative Cognitive Dysfunction

Bohan Lin[#], Wei Liu[#], Xiu Ni and Fuyi Shen[*]

Department of Anesthesiology, Shanghai First Maternity and Infant Hospital, School of Medicine, Tongji University, Shanghai, China
*Corresponding Author: Fuyi Shen. Email: shenfuyi315315@hotmail.com
[#]These authors are the co-first authors

Received: 09 December 2025; Accepted: 04 March 2026; Published: 09 June 2026

ABSTRACT: Background: Postoperative cognitive dysfunction (POCD) is a common neurological complication in elderly patients. However, the mechanism by which glutamate ionotropic receptor NMDA type subunit 2B (GluN2B) contributes to POCD development remains incompletely understood. This study aimed to investigate the effects of GluN2B overexpression on POCD improvement and elucidate its underlying molecular mechanisms. **Methods:** *In vitro*, lipopolysaccharide (LPS) was used to induce inflammation in mouse primary microglia, and a microglia-HT22 neuron co-culture system was established to simulate the neurotoxic environment. Overexpression and knockdown constructs for GluN2B and brain-derived neurotrophic factor (BDNF) were generated. Western blot, ELISA, immunofluorescence, and flow cytometry were employed to assess GluN2B expression, BDNF/tropomyosin receptor kinase B (TrkB) signaling proteins, microglial M1/M2 polarization markers, neuronal apoptosis, and synaptic markers. *In vivo*, an aged mouse POCD model was established to evaluate the effects of GluN2B overexpression on cognitive function, neuroinflammation, and neural injury markers. **Results:** LPS treatment downregulated GluN2B expression in microglia (4.71-fold, $p < 0.001$), promoted polarization toward the pro-inflammatory M1 phenotype, and suppressed the BDNF/TrkB pathway. GluN2B overexpression significantly reversed these effects by inhibiting M1 polarization, enhancing anti-inflammatory M2 polarization, and activating BDNF/TrkB signaling. In the microglia-HT22 co-culture system, GluN2B overexpression markedly attenuated LPS-activated microglia-induced neuronal apoptosis (1.74-fold, $p < 0.001$), intracellular Ca^{2+} overload (1.94-fold, $p < 0.001$), and synaptic protein loss in HT22 cells, whereas BDNF knockdown abolished these protective effects. In the aged POCD mouse model, GluN2B overexpression improved learning and memory performance and reduced neuronal apoptosis (1.92-fold, $p < 0.001$) and histopathological damage in the prefrontal cortex. **Conclusion:** This study demonstrates that GluN2B overexpression activates the BDNF/TrkB pathway to reduce neuroinflammation, protect neurons and synapses, and ameliorate POCD symptoms in aged mice, providing a potential therapeutic target for POCD management.

KEYWORDS: Glutamate ionotropic receptor NMDA type subunit 2B; brain-derived neurotrophic factor/tropomyosin receptor kinase B pathway; postoperative cognitive dysfunction; microglial polarization; neuroinflammation

1 Introduction

Postoperative Cognitive Dysfunction (POCD) is a frequent complication affecting the nervous system after surgery. It disproportionately impacts elderly patients, in whom it is associated with a poorer prognosis [1–3]. POCD significantly impedes recovery and quality of life by causing persistent cognitive deficits in memory, attention, and executive function [4]. Although the clinical significance of POCD has been widely

recognized, its precise pathogenesis remains incompletely elucidated. In recent years, neuroinflammation has been established as a critical contributor to the development and progression of POCD [5,6]. Surgical trauma and anesthetic stress trigger systemic inflammation and disrupt the Blood–Brain Barrier (BBB). This disruption allows peripheral inflammatory mediators to enter the brain and activate microglia and astrocytes in key cognitive regions such as the hippocampus [7]. These activated glial cells release large amounts of pro-inflammatory cytokines, creating a sustained neuroinflammatory microenvironment. This milieu directly damages neuronal structure and function, disrupts synaptic activity, and ultimately contributes to cognitive impairment [8–10]. Therefore, effectively suppressing or modulating postoperative neuroinflammation is a crucial strategy for preventing and treating POCD.

N-methyl-D-aspartate receptors (NMDARs) play a pivotal role in the central nervous system (CNS) by mediating excitatory synaptic transmission and forms of plasticity like long-term potentiation (LTP), mechanisms that are fundamental to learning and memory [11,12]. NMDARs consist of various subunits, among which the glutamate ionotropic receptor NMDA type subunit 2B (GluN2B) subunit is highly enriched in the hippocampus and prefrontal cortex (PFC) [13,14]. Abnormalities in the expression level, subcellular localization, and phosphorylation status of GluN2B are closely associated with the pathological processes of multiple cognitive disorders [15,16]. GluN2B not only determines receptor kinetic properties but also serves as a crucial hub connecting synaptic function and signal transduction networks through its large intracellular C-terminal domain [17]. Central to POCD pathology is the disruption of synaptic structure and functional plasticity [18]. Conversely, the Brain-derived neurotrophic factor (BDNF)-tropomyosin receptor kinase B (TrkB) axis, a vital pathway for sustaining neuronal survival, differentiation, and synaptic plasticity, offers significant neuroprotective benefits [19]. Initiation of BDNF/TrkB signaling effectively counteracts neuroinflammatory damage, inhibits excessive glial activation, and promotes neuronal repair and regeneration [20]. Importantly, there exists a precise bidirectional regulatory relationship between the BDNF/TrkB pathway and GluN2B function. Evidence indicates that BDNF activates TrkB, triggering downstream signaling cascades such as protein kinase C (PKC) and proline-rich tyrosine kinase 2 (Pyk2), which facilitate the trafficking and anchoring of GluN2B subunits to the postsynaptic membrane. This enhances NMDAR-mediated synaptic currents and LTP, thereby mediating neural plasticity [21]. Therefore, modulating the BDNF/TrkB-GluN2B signaling axis not only helps maintain synaptic function stability but may also serve as a potential therapeutic target for preventing and treating POCD.

Previous animal and clinical studies have suggested that NMDAR dysfunction is closely associated with synaptic plasticity impairment and cognitive deficits related to POCD [22], and other reports have shown that downregulation of the BDNF/TrkB signaling pathway correlates with cognitive decline in POCD model mice [23]. However, most studies have examined single molecules or individual pathways in isolation, and there is a lack of work that integratively analyzes GluN2B, BDNF/TrkB signaling, and the neuroinflammatory state within a unified framework and establishes their causal relationships. Building on these prior findings, the present study aims to systematically evaluate, from the perspective of an integrated "GluN2B–BDNF/TrkB–neuroinflammation" signaling axis, the role of this axis and the interactions among its components in the onset and progression of POCD. Based on the above, this study aims to systematically investigate whether targeted overexpression of GluN2B in the hippocampus can ameliorate POCD-related cognitive and behavioral deficits. To this end, we established both animal and cellular models and applied gene overexpression techniques. We further intend to elucidate the underlying molecular mechanisms, focusing on the activation effect of GluN2B overexpression on the BDNF/TrkB signaling pathway and its regulatory role in neuroinflammation. This research seeks to define the contribution

of the GluN2B-BDNF/TrkB-Neuroinflammation axis to POCD pathogenesis. The findings are expected to reveal new therapeutic targets and inform the rationale for strategies to prevent and treat POCD.

2 Materials and Methods

2.1 Cell Culture and Transfection

Primary microglial cells were isolated from mice following previously reported methods [24]. Whole brains were harvested from 1- to 2-day-old neonatal C57BL/6 mice (6 mice, both sexes), obtained from the Suzhou University Laboratory Animal Center, and reared under specific pathogen-free (SPF) conditions. The neonatal mice were euthanized by rapid decapitation before brain collection. The brains were washed in ice-cold PBS (0.01 M, pH 7.2), and the cerebral cortices were carefully dissected. The tissue was gently triturated in DMEM (Gibco, 11965092; Grand Island, NY, USA) supplemented with 10% FBS (Gibco, A5256701) and 1% antibiotic-antimycotic (Beyotime, C0222, Shanghai, China). The cell suspension was filtered through a 100 μm cell strainer (NEST, 258367, Wuxi, China) and centrifuged (Eppendorf 5424 R, Hamburg, Germany) at 1000 rpm for 5 min at 4°C. The pellet was resuspended in DMEM and cultured for 10–14 days in a Midi CO_2 incubator (Thermo, Waltham, MA, USA). The culture was shaken at 120 rpm for 4 h to induce microglial detachment, and the supernatant containing microglial cells was collected. Microglial identity was confirmed by immunofluorescence staining. HT22 cells (CC-Y2137) were obtained from EK-Bioscience (Shanghai, China), authenticated by short tandem repeat (STR) profiling, and routinely tested to confirm the absence of mycoplasma contamination.

Lipofectamine 3000 (Invitrogen, L3000150, Carlsbad, CA, USA) was used to transfect siRNA (si-GluN2B, si-BDNF, si-NC) or overexpression vectors (oe-GluN2B, oe-NC) into microglia [25]. After 6 h of transfection, the medium was replaced, and cells were harvested for Western blot validation 48 h later. Transfection efficiency was assessed by measuring the expression levels of corresponding proteins via Western blot. si-GluN2B, si-BDNF (5′-CGGTCACAGTCCTTGAAAA-3′), si-NC, oe-GluN2B, and oe-NC were synthesized by GenePharma (Shanghai, China).

2.2 Cell Treatments

To determine the optimal LPS concentration for inducing inflammatory responses in microglial cells, cells were co-incubated with LPS (1/10/25/50/100/200 ng/mL; MCE, HY-D1056, Monmouth Junction, NJ, USA) for 24 h. Cell viability was assessed to identify the LPS concentration that elicited significant inflammatory responses without causing severe cytotoxicity. Subsequently, eight experimental groups were established to investigate the role of GluN2B in regulating neuroinflammation: (1) Control group, negative control; (2) LPS group, treated with 10 ng/mL LPS for 24 h; (3) LPS + si-NC group, cells transfected followed by LPS treatment; (4) LPS + si-GluN2B group; (5) LPS + oe-NC group; (6) LPS + oe-GluN2B group; (7) LPS + oe-GluN2B + si-NC group, cells co-transfected with oe-GluN2B and si-NC followed by LPS treatment; (8) LPS + oe-GluN2B + si-BDNF group.

To evaluate the effect of activated microglia on neurons, microglial cells were co-cultured with HT22 neuronal cells using a Transwell system. HT22 cells (5×10^4 cells/well) were seeded at the bottom of 6-well plates, while microglia were seeded in Transwell chambers (NEST, 723101). After establishing the co-culture system, microglia were treated with LPS (10 ng/mL) or transfected according to experimental grouping and co-cultured for 48 h. During co-culture, cytokines released by microglia could pass through the Transwell membrane to influence HT22 neurons, while the cells themselves did not have direct contact.

2.3 Cell Viability

Microglial cells (5×10^3 cells/well) were seeded in 96-well plates and treated according to the experimental design. After treatment, 10 μL of CCK-8 solution (Yesen, 40203ES, Shanghai, China) was added to each well and incubated in an incubator for 2.5 h. Optical density (OD) values were measured at 450 nm using a microplate reader (BioTek, ELx808, Winooski, VT, USA) to assess cell viability [26].

2.4 Lactate Dehydrogenase (LDH) Assay for Neuronal Cell Damage

An LDH cytotoxicity detection kit (Meilunbio, MA0649, Dalian, China) was used to measure LDH release to evaluate HT22 neuronal cell damage. After treatment, culture supernatants were collected and incubated with the LDH detection working solution for 10 min. Following the addition of the stop solution, absorbance was measured at 490 nm using a microplate reader (Thermo, Multiskan FC). The amount of LDH released is positively correlated with the degree of cell damage.

2.5 Calcein-Acetoxymethyl Ester (AM)/Propidium Iodide (PI) Staining

The viability of HT22 neuronal cells was assessed using a Calcein-AM/PI double staining kit (Meilunbio, MA0361). After treatment, cells were washed with PBS (0.01 M, pH 7.2) and incubated with 1 μM Calcein-AM and 1 μM PI working solution for 20 min. Cells were observed under a microscope (Zeiss, Observer Z1, Oberkochen, Germany). Live cells stained with Calcein-AM exhibited green fluorescence, while dead or membrane-compromised cells stained with PI exhibited red fluorescence.

2.6 Intracellular Ca^{2+} Level Measurement

Intracellular Ca^{2+} concentration in HT22 cells was measured using the fluorescent probe Fura-2/AM (MCE, HY-101897). After treatment, cells were incubated with culture medium containing 10 μmol/L Fura-2/AM for 30 min. Following excitation at 340 nm and 380 nm, fluorescence emission at approximately 505 nm was captured by fluorescence microscopy (Olympus, FV3000, Tokyo, Japan). The ratio of fluorescence intensities (F340/F380) was then calculated to represent fluctuations in intracellular Ca^{2+} concentration.

2.7 Flow Cytometry

Apoptosis of microglial cells and HT22 cells was detected by Annexin V-APC/PI double staining. After the treatments described in Section 2.2 were completed, cells were harvested and resuspended at 1×10^6 cells/mL, then incubated with Annexin V-APC and PI staining solution (Invitrogen, 88-8007-74) for 15 min. The binding buffer was then added, and the samples were analyzed using a flow cytometer (Becton Dickinson, BD FACSCanto II, Franklin Lakes, NJ, USA). Data were analyzed with FlowJo software (version 7.6.1, FlowJo LLC, Ashland, OR, USA) to determine the apoptotic rate.

2.8 Animals

Eighteen-month-old male C57BL/6J mice (weighing 25–30 g) were purchased from Ensville Biotechnology Co., Ltd. (Chengdu, China). Mice were acclimated for one week under standard environmental conditions with ad libitum access to food and water. All animal experiments were approved by the Shanghai First Maternity and Infant Hospital, School of Medicine, Tongji University Ethics Committee (NO. TJBG10522101).

In this study, 36 mice were randomly divided into four groups (n = 9 per group): Sham, POCD, POCD + oe-NC, and POCD + oe-GluN2B. The POCD animal model was established via isoflurane anesthesia combined with exploratory laparotomy [27]. Mice were initially anesthetized in a chamber containing

3% isoflurane and oxygen, then maintained under 1.5% isoflurane and oxygen during surgery. A midline abdominal incision approximately 1 cm in length was made, after which about 10 cm of the intestine was externalized and maintained outside the peritoneal cavity for 2 min. The peritoneum and skin were sutured using sterile 4-0 chromic gut sutures. Surgery lasted 30 min. Control mice underwent no anesthesia or surgery. Behavioral testing was conducted 24 h postoperatively, and brain tissues were collected 48 h after surgery and stored at −80°C.

To overexpress GluN2B in the PFC of POCD model mice, lentivirus-mediated oe-GluN2B (titer 1×10^9 TU/mL, 2 μL; pcSLenti-EGFP-CMV-Grin2b, Obio Technology, Shanghai, China) was stereotactically injected into the PFC. Injections were performed using a Hamilton syringe at a rate of 0.2 μL/min. After injection, the syringe was left in place for 5 min to facilitate viral diffusion. Mice were returned to their cages for recovery for at least one week before behavioral testing and tissue collection.

2.9 Behavioral Tests

2.9.1 Morris Water Maze Test

Spatial learning and memory in mice were evaluated using the Morris water maze [28]. The apparatus consisted of a circular tank (diameter: 120 cm, depth: 30 cm) containing tap water mixed with non-toxic white paint to obscure the submerged platform. Water temperature was kept constant at 22 ± 1°C throughout testing. A circular escape platform (10 cm diameter) was positioned within the pool, and the arena was conceptually divided into four quadrants relative to platform placement: target, opposite, left, and right. The testing protocol comprised three sequential phases. During the initial cued phase (3 days, 4 trials daily, 15-min inter-trial intervals), a visible flag marked the platform location, which varied randomly across trials along with entry points. Each trial lasted up to 60 s, after which mice unable to locate the platform were manually guided to it and allowed to remain for 10 s. Between trials, mice were warmed under a heat lamp to prevent hypothermia. Following a 48-h rest period, the acquisition phase commenced (5 days, 4 trials daily, 15-min intervals). The platform position was now fixed, the flag removed, and additional proximal cues were placed around the pool perimeter. Trial procedures otherwise remained consistent with the cued phase. Memory retention was evaluated 24 h post-acquisition via a single 60-s probe trial. The platform was removed, and mice entered from a novel location opposite to the former platform position. The ANY-Maze video tracking system (Stoelting Co., Wood Dale, IL, USA) recorded escape latency, swimming velocity, and time spent in each quadrant.

2.9.2 Fear Conditioning Test

Associative memory was assessed through fear conditioning [29], which included both training and testing sessions. During training, mice were placed in the conditioning chamber (StartFear system, Panlab, Barcelona, Spain) and allowed a 2-min acclimation period, followed by an auditory stimulus (80 dB, 2.8 kHz, 30 s) paired with a foot shock (0.75 mA, 2 s). This procedure was repeated twice with a 2-min interval between shocks. Mice were removed 30 s after the second shock. Testing occurred 24 h later by placing mice back into the same chamber for 5 min without any stimuli; freezing behavior duration (%) was recorded. Freezing behavior, defined as complete immobility except for respiration, was analyzed using Time FZ2 software (O'Hara & Co., Tokyo, Japan).

2.9.3 Y-Maze Test

The Y-maze test assessed spatial working memory [23]. The Y-maze apparatus (manufactured by Zhangjiagang Teaching Experimental Instrument Factory, China) consists of three arms (35 cm in length,

10 cm in width, and 20 cm in height) arranged at 120° angles to each other. Each arm is equipped with an LED light at its distal end. The shocks are delivered as 0.5-s pulses, current-controlled (maximum output voltage < 30 V, 0.2–0.8 mA), repeated every 2 s, until the mouse enters the safe arm or 10 s have passed. After a 3-min acclimation period, the experiment begins. At the start of each trial, one arm is randomly selected as the safe arm using a computer-generated random sequence, and the corresponding light is illuminated, while the other two arms are designated as shock arms (shock applied after 2 s). The experimenter conducting the test is blinded to the group allocation. A trial is considered successful if the mouse enters and remains in the lit arm (with all four paws inside) within 10 s. The experiment continues after each shock until the mouse stays in the safe zone for 15 consecutive seconds. After each trial, feces and urine are cleaned, and the maze walls are wiped with 75% ethanol to remove odors. If the mouse achieves 9 successes in 10 consecutive shocks, it is considered to have reached the learning criterion. The number of shocks the mouse received before reaching the criterion is recorded.

2.9.4 Novel Object Recognition (NOR) Test

The NOR test evaluated recognition memory [30]. The experiment consisted of a training phase and a testing phase. Mice were first habituated to the empty arena (50 cm × 50 cm × 50 cm) for 10 min per day for two consecutive days to familiarize them with the environment. Training phase: Mice were placed in an open-field arena containing two identical objects and allowed to freely explore for 10 min. At the end of training, the apparatus and arena were thoroughly cleaned with 75% ethanol. Testing phase: After a 24-h interval, one of the familiar objects was replaced with a novel object, and the mice were allowed to explore for another 10 min. The time spent interacting with the novel object was quantified using EthoVision XT 16 (Noldus Information Technology, Wageningen, The Netherlands) equipped with a deep-learning-based tracking algorithm. The software tracked the position of the mouse's nose and calculated the time spent within 2 cm of the object's outer contour. The time spent exploring the novel and familiar objects was recorded, and the preference for the novel object was calculated as: exploration time for novel object/(exploration time for novel + familiar objects).

2.10 HE Staining and Nissl Staining

After euthanasia, mouse brain tissues were collected, fixed in 4% PFA for 24 h, embedded in paraffin, and sectioned continuously at 5 μm thickness. Sections were first deparaffinized in xylene (two changes, 15 min each) and rehydrated through a descending alcohol series (100%, 95%, 85%, and 75% ethanol, 5 min each). The sections were then stained with hematoxylin (Aladdin, 517-28-2, Shanghai, China) for 2 min, rinsed in running tap water for 10 min, differentiated in 1% acid alcohol for 3 min, and counterstained with eosin (Aladdin, E774785) for 1 min. After rinsing with distilled water and air-drying, the sections were dehydrated in absolute ethanol for 1 min, cleared in xylene for 10 min, and mounted with neutral balsam mounting medium (BL704A, Biosharp, Hefei, China). Neuronal morphology and arrangement in the prefrontal cortex of the mouse brain were examined using a light microscope (BX53, Olympus, Tokyo, Japan).

Nissl staining was performed using a Nissl staining kit (Solarbio, G1434, Beijing, China) to evaluate neuronal number and morphology in the PFC. After dewaxing and hydration, 5 μm brain sections were stained with methylene blue solution (provided in the commercial kit) at 37°C for 1 h, differentiated in Nissl differentiation solution for 3 min to clearly visualize Nissl bodies, treated with ammonium molybdate solution (provided in the commercial kit) for 3 min, washed, and mounted. Nissl bodies and neuronal counts were observed under a light microscope.

2.11 TUNEL Staining

Paraffin-embedded brain tissue sections (5 μm) were dewaxed, hydrated, and treated with proteinase K (10 mg/mL, Solarbio, P9460) for 20 min. Sections were incubated with TUNEL detection solution (Vazyme, A113-01, Nanjing, China) for 1 h. Subsequently, slices were incubated with DAPI (1 μg/mL, Beyotime, C1002; Shanghai, China) for 5 min and observed under a fluorescence microscope to quantify the percentage of apoptotic cells.

2.12 ELISA

To measure relevant cytokine levels in the mouse PFC, collected brain tissue samples were thoroughly homogenized and centrifuged at 5000× *g* (10 min, 4°C) to obtain supernatants. After microglial cell treatment, culture supernatants were collected. ELISA kits were used to detect TNF-α (MyBioSource, MBS9711588, San Diego, CA, USA), IL-6 (MyBioSource, MBS3805296), IL-10 (MyBioSource, MBS286979), and Arg-1 (MyBioSource, MBS3805532) according to the manufacturer's protocols. Absorbance was measured at 450 nm using a microplate reader, and cytokine concentrations were calculated based on standard curves.

2.13 Immunofluorescence

After the treatments described in Section 2.2 were completed, cells (microglial cells and HT22 cells) were fixed with 4% PFA, permeabilized with 0.3% Triton X-100, and blocked with 5% goat serum. Paraffin-embedded mouse brain tissue sections were dewaxed, hydrated, subjected to antigen retrieval, and blocked. Subsequently, cells or tissue sections were incubated overnight at 4°C with primary antibodies including Iba1 (1:100, Bioss, bs-1363R; Beijing, China), Transmembrane Protein 119 (TMEM119, 1:200, CST, #90840; Danvers, MA, USA), Purinergic Receptor P2Y12 (P2RY12, 1:2000, CST, #69766), GluN2B (1:300, GeneTex, GTX109713; Irvine, CA, USA), CD86 (1:100, Bioss, bs-1035R), Synaptophysin (SYP, 1:300, Bioss, bsm-52379R), PSD-95 (1:200, Bioss, bs-0179R), and CD206 (1:500, CST, #24595). On the following day, samples were incubated for 1 h with fluorescent secondary antibodies (1:200, Bioss, bs-0295G-BF488/bs-0295G-BF594), washed, and stained with DAPI (1 μg/mL) for 5 min. Fluorescence microscopy was used for observation and imaging.

Dual immunofluorescence staining of Iba1 with TMEM119 and P2RY12 was employed to identify microglia. Co-staining of Iba1 and CD86 was used to evaluate M1 microglial activation. Co-staining of SYP and PSD-95 assessed synaptic integrity and density in HT22 cells. In mouse brain tissue, Iba1/CD86 co-staining evaluated M1 microglia, while Iba1/CD206 co-staining assessed M2 microglia.

2.14 Western Blot

After the treatments described in Section 2.2 were completed, microglial cells or HT22 cells were collected and lysed with RIPA buffer (Beyotime, P0013). Following euthanasia, PFC tissues from mice were also homogenized and lysed using RIPA buffer. Protein concentration was determined by the BCA assay (Beyotime, P0010). Equal amounts of protein samples were subjected to SDS-PAGE gel electrophoresis and subsequently transferred onto PVDF membranes. Membranes were blocked with 5% non-fat milk and incubated overnight at 4°C with primary antibodies against GluN2B (1:1000, CST, #4207), CD86 (1:500, Bioss, bs-1035R), iNOS (1:2000, Bioss, bs-0162R), CD206 (1:1000, CST, #24595), Arg-1 (1:500, GeneTex, GTX109242), BDNF (1:500, Bioss, bs-4989R), p-TrkB (1:1000, Bioss, bsm-52213R), TrkB (1:1000, Bioss, bsm-61083R), BAX (1:2000, Bioss, bsm-52316R), BCL2 (1:3000, Bioss, bsm-61074R), PSD-95 (1:500, Bioss, bs-0179R), SYP (1:5000, Bioss, bsm-52379R), and GAPDH (1:10000, Bioss, bs-10900R). The following day, membranes were washed with TBST and incubated for 1 h with HRP-conjugated secondary antibodies (1:20000, Bioss, bs-0295G-HRP). Protein bands were visualized using ECL reagent (Beyotime, P0018) and imaged with a

Tanon 5200 chemiluminescent imaging system (Shanghai, China). GAPDH served as the internal control for quantitative analysis of target protein expression.

2.15 Statistical Analyses

Statistical analyses were performed using SPSS 26.0 (IBM SPSS, Chicago, IL, USA). Data were expressed as mean ± standard deviation. For animal experiments, each group included n = 9 mice. Cell experiments were independently repeated six times, with five replicate wells in each independent experiment, and the mean value of the replicates was used for statistical analysis. Prior to statistical analyses, data normality was assessed using the Shapiro–Wilk test, and homogeneity of variances was evaluated using Levene's test. Differences between the two groups were assessed using independent samples *t*-tests. Comparisons among multiple groups were analyzed by one-way ANOVA followed by Bonferroni post hoc correction. A *p*-value less than 0.05 was considered statistically significant.

3 Results

3.1 Downregulation of GluN2B in LPS-Induced Microglia

To investigate the role of GluN2B in neuroinflammation, primary microglia were first isolated and identified from mice. Iba1, TMEM119, and P2RY12 are commonly used as specific markers for microglia [31]. Immunofluorescence results showed that the isolated microglial cells were all positive for Iba1 and exhibited double-positive staining for TMEM119 and P2RY12 (Fig. 1A,B). To establish a microglial injury and inflammation model, the induction concentration of LPS was screened using the CCK-8 assay. Ultimately, treatment with 10 ng/mL LPS for 24 h was selected for subsequent experiments (Fig. 1C). LPS treatment increased the apoptosis rate of microglia (Fig. 1D,E). Immunofluorescence results showed that the fluorescence intensity of GluN2B in the LPS-treated group was markedly decreased compared to the Control group (Fig. 1F,G). LPS treatment significantly reduced the protein expression levels of GluN2B in microglia (Fig. 1H,I). These results suggest that LPS (10 ng/mL, 24 h) successfully induces apoptosis in primary microglia and significantly downregulates GluN2B expression during this process.

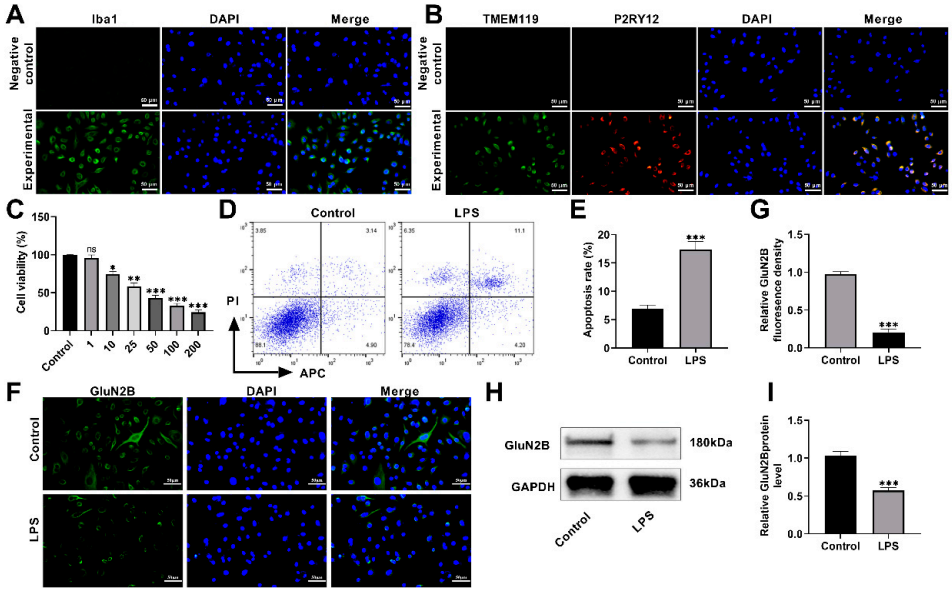

Figure 1: Downregulation of GluN2B in LPS-induced microglia. (**A**) Identification of isolated primary microglia by Iba1 immunofluorescence staining. Negative control: HT22 neuronal cells. Experimental: primary microglia. Scale

bar: 50 μm. (**B**) Further microglial identification via dual immunofluorescence staining of TMEM119 and P2RY12. Negative control: HT22 neuronal cells. Experimental: primary microglia. Scale bar: 50 μm. (**C**) Different concentrations of LPS treatments were applied (1/10/25/50/100/200 ng/mL). The CCK-8 assay was used to screen for an appropriate LPS concentration to induce microglial injury; 10 ng/mL LPS treatment for 24 h was selected as the experimental condition. (**D**,**E**) Flow cytometry assessed cell apoptosis to analyze the effects of LPS on microglial apoptosis. (**F**,**G**) Immunofluorescence staining detected intracellular changes in GluN2B protein expression. Scale bar: 50 μm. (**H**,**I**) GluN2B protein levels. n = 6. ns $p > 0.05$, $^{*}p < 0.05$, $^{**}p < 0.01$, $^{***}p < 0.001$ vs. Control.

3.2 Overexpression of GluN2B Inhibits LPS-Induced Microglial Activation and Pro-Inflammatory Phenotype

To explore the function of GluN2B in microglial activation, the knockdown and overexpression efficiency of GluN2B by si-GluN2B and oe-GluN2B were first verified by Western blot (Fig. 2A,B). Through optical microscopy observation and CCK-8 assay, it was found that LPS treatment led to decreased viability of microglial cells (Fig. 2C,D). However, under LPS conditions, si-GluN2B further exacerbated the LPS-induced reduction in cell viability. In contrast, compared with the oe-NC group, oe-GluN2B was able to reverse the LPS-induced decrease in cell viability, demonstrating a protective effect after LPS treatment.

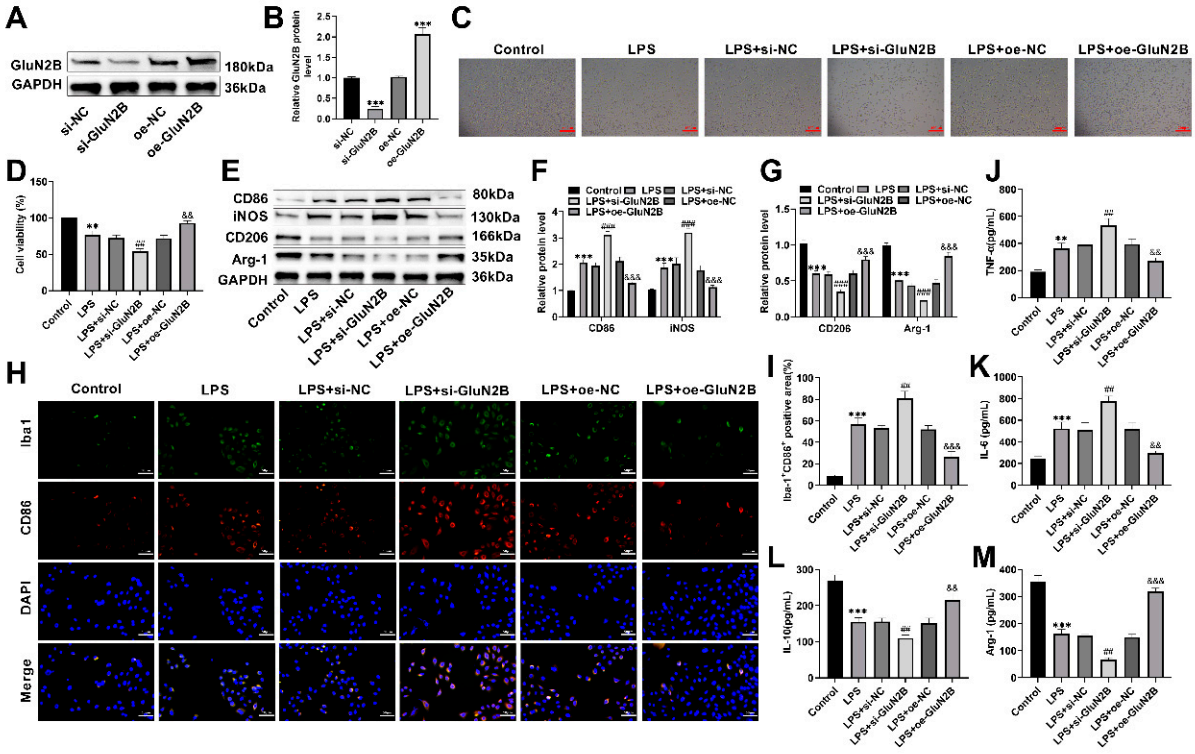

Figure 2: Overexpression of GluN2B inhibits LPS-induced microglial activation and pro-inflammatory phenotype. (**A**,**B**) Western blot validation of si-GluN2B and oe-GluN2B transfection efficiency. $^{***}p < 0.001$ vs. NC. (**C**) Morphological changes observed with optical microscopy. Scale bar: 200 μm. (**D**) Cell viability measured by CCK-8 assay. (**E**–**G**) Western blot detection of macrophage M1 polarization markers CD86, iNOS, and M2 polarization markers CD206, Arg-1. (**H**,**I**) Immunofluorescence analysis of co-expression of microglial marker Iba1 and pro-inflammatory marker CD86. Scale bar: 50 μm. (**J**–**M**) ELISA quantification of TNF-α, IL-6, IL-10, Arg-1 levels. n = 6. $^{**}p < 0.01$, $^{***}p < 0.001$ vs. Control; $^{\#\#}p < 0.01$, $^{\#\#\#}p < 0.001$ vs. LPS + si-NC; $^{\&\&}p < 0.01$, $^{\&\&\&}p < 0.001$ vs. LPS + oe-NC.

To further elucidate the regulatory role of GluN2B on inflammatory phenotypes, M1 and M2 polarization markers were analyzed. Western blot results demonstrated that LPS stimulation significantly upregulated M1 markers CD86 and iNOS protein levels, while downregulating M2 markers CD206 and Arg-1 expression (Fig. 2E–G). Knockdown of GluN2B further enhanced M1 marker expression and reduced M2 marker protein levels. In contrast, overexpression of GluN2B effectively reversed these changes, significantly inhibiting M1 polarization and promoting M2 polarization. Moreover, ELISA measurements of cytokines revealed that LPS stimulation markedly increased pro-inflammatory factors while suppressing anti-inflammatory factors (Fig. 2J–M). Immunofluorescence results revealed that LPS induction significantly increased the number of M1 microglia ($Iba1^+CD86^+$), and knockdown of GluN2B further enhanced microglial M1 polarization. Conversely, overexpression of GluN2B effectively reversed these changes, significantly inhibiting M1 polarization (Fig. 2H,I). Overexpression of GluN2B significantly decreased pro-inflammatory cytokine levels and increased anti-inflammatory cytokine levels. These findings indicate that overexpression of GluN2B effectively inhibits LPS-induced pro-inflammatory M1 activation of microglia and promotes their conversion to an anti-inflammatory M2 phenotype, thereby exerting anti-inflammatory and protective effects.

3.3 Overexpression of GluN2B Ameliorates LPS-Induced Microglial Activation-Mediated Neural Injury

To investigate the indirect neurotoxic effects of microglial activation and the modulatory role of GluN2B, a co-culture system of microglia and HT22 neuronal cells was established. The results demonstrated that co-culture with LPS-activated microglia significantly exacerbated HT22 neuronal damage, as evidenced by a marked increase in LDH release (Fig. 3A). Calcein-AM/PI staining revealed a reduction in live cells (green fluorescence) and an increase in dead cells (red fluorescence) in the LPS group (Fig. 3B,C). Flow cytometry further confirmed that co-culture under LPS conditions significantly elevated the apoptosis rate of HT22 neurons (Fig. 3D,E). Moreover, si-GluN2B promoted LDH release, increased the proportion of dead HT22 cells, and induced apoptosis. Conversely, oe-GluN2B) significantly improved neuronal survival and inhibited apoptosis. Intracellular calcium overload is a key trigger of apoptosis. Fura-2/AM calcium imaging showed that LPS-activated co-culture caused a significant elevation of intracellular Ca^{2+} in HT22 cells, indicating disrupted neuronal calcium homeostasis. In contrast, GluN2B overexpression significantly restored Ca^{2+} levels (Fig. 3F,G).

To assess synaptic structural integrity, expression of key synaptic proteins was examined. Immunofluorescence analysis showed significantly decreased fluorescence intensity of synaptic markers SYP and PSD-95 in HT22 cells from the LPS group (Fig. 3H–J). si-GluN2B further reduced synaptic marker expression, while GluN2B overexpression effectively reversed this reduction. Additionally, LPS co-culture markedly upregulated the pro-apoptotic protein BAX, downregulated the anti-apoptotic protein BCL-2, and decreased PSD-95 and SYP protein levels in HT22 cells; overexpression of GluN2B significantly reversed these protein expression changes (Fig. 3K–M). These findings suggest that GluN2B overexpression mitigates indirect neurotoxicity mediated by microglial activation by inhibiting neuronal death, restoring calcium homeostasis, and alleviating synaptic damage, thereby exerting a neuroprotective effect.

3.4 GluN2B Regulates the BDNF/TrkB Pathway

In microglia, Western blot analysis was conducted to evaluate the effects of LPS treatment and GluN2B overexpression on the expression and phosphorylation levels of key proteins in the BDNF/TrkB pathway. Results showed that LPS significantly downregulated BDNF protein expression and phosphorylation of the TrkB receptor, indicating that LPS-induced neuroinflammation suppresses the BDNF/TrkB signaling pathway (Fig. 4A–C). si-GluN2B elicited effects similar to LPS, further exacerbating pathway inhibition;

in contrast, oe-GluN2B effectively reversed LPS-induced suppression, significantly enhancing levels of BDNF and phosphorylated TrkB.

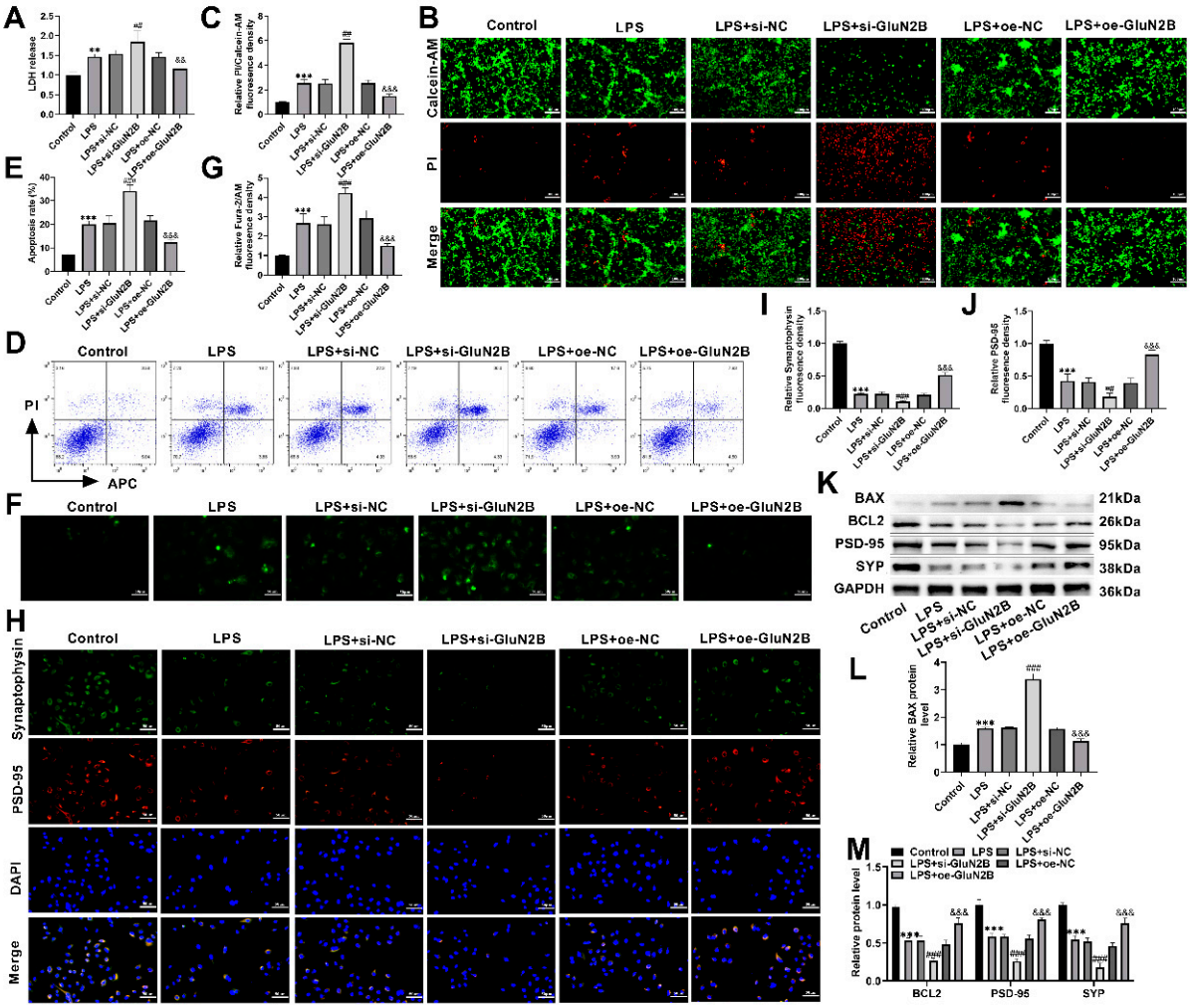

Figure 3: Overexpression of GluN2B ameliorates neurotoxicity mediated by LPS-induced microglial activation. (**A**) Assessment of HT22 neuronal injury by LDH release assay. (**B**,**C**) Calcein-AM/PI staining evaluated HT22 cell survival status (green: live cells; red: dead cells). Scale bar: 100 μm. (**D**,**E**) Flow cytometry measured apoptotic proportions of HT22 cells. (**F**,**G**) Intracellular Ca^{2+} concentration in HT22 cells was detected using Fura-2/AM probe. Scale bar: 50 μm. (**H**–**J**) Immunofluorescence analysis of SYP and PSD-95 expression. Scale bar: 50 μm. (**K**–**M**) Western blot detection of apoptosis-related proteins (BAX, BCL2) and synaptic marker proteins (PSD-95, SYP) in HT22 cells. n = 6. $^{**}p < 0.01$, $^{***}p < 0.001$ vs. Control; $^{\#\#}p < 0.01$, $^{\#\#\#}p < 0.001$ vs. LPS + si-NC; $^{\&\&}p < 0.01$, $^{\&\&\&}p < 0.001$ vs. LPS + oe-NC.

To confirm whether BDNF is a critical downstream effector mediating GluN2B's function, knockdown experiments were performed in cells overexpressing GluN2B. Results demonstrated that si-BDNF successfully reduced BDNF protein expression (Fig. 4D,E). Notably, under GluN2B overexpression conditions, BDNF knockdown (LPS + oe-GluN2B + si-BDNF) significantly reversed the upregulation of BDNF and TrkB phosphorylation induced by GluN2B overexpression (Fig. 4F–H). In summary, GluN2B overexpression antagonizes LPS-induced inhibition of the BDNF/TrkB signaling pathway, and this protective effect is significantly attenuated by BDNF knockdown, confirming BDNF as a key downstream effector of GluN2B.

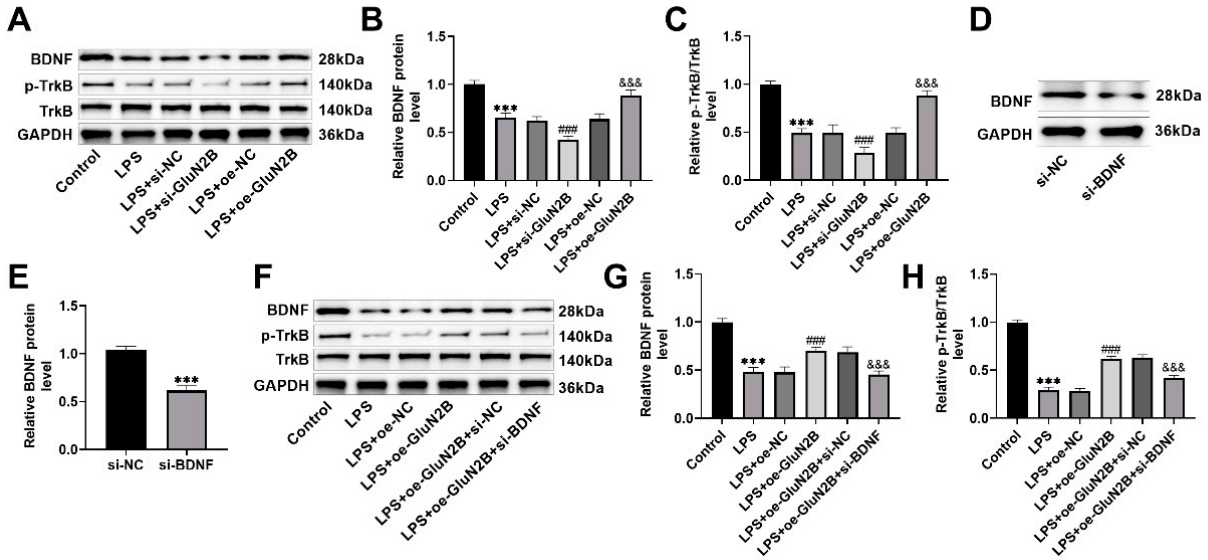

Figure 4: Regulation of the BDNF/TrkB pathway by GluN2B. (**A**–**C**) Western blot analysis of BDNF, p-TrkB, and total TrkB protein expression. $^{***}p < 0.001$ vs. Control; $^{###}p < 0.001$ vs. LPS + si-NC; $^{\&\&\&}p < 0.001$ vs. LPS + oe-NC. (**D**,**E**) Western blot verification of si-BDNF transfection efficiency. $^{***}p < 0.001$ vs. si-NC. (**F**–**H**) Western blot detection of expression changes in BDNF, p-TrkB, and TrkB proteins. n = 6. $^{***}p < 0.001$ vs. Control; $^{###}p < 0.001$ vs. LPS + oe-NC; $^{\&\&\&}p < 0.001$ vs. LPS + oe-GluN2B + si-NC.

3.5 GluN2B Regulates BDNF/TrkB Signaling to Ameliorate LPS-Induced Neuroinflammation, Neuronal Injury, and Synaptic Dysfunction

To elucidate the key molecular role of BDNF in the neuroprotective effects of GluN2B, this study conducted rescue experiments for validation. Immunofluorescence analysis showed that LPS stimulation markedly increased the proportion of cells co-expressing Iba1 (green) and the M1 phenotype marker CD86 (red), indicating enhanced microglial M1 polarization. Overexpression of GluN2B (LPS + oe-GluN2B) significantly reduced the percentage of $Iba1^{+}CD86^{+}$ cells, whereas the inhibitory effect of GluN2B overexpression on microglial M1 polarization was notably attenuated when BDNF was simultaneously knocked down (LPS + oe-GluN2B + si-BDNF) (Fig. 5A,B). Western blot assays corroborated this trend. LPS markedly upregulated protein levels of M1 markers (CD86, iNOS) and downregulated M2 markers (CD206, Arg-1) (Fig. 5C–E). Overexpression of GluN2B reversed the abnormal expression of these inflammatory markers, but the knockdown of BDNF abrogated the effects of oe-GluN2B.

At the neuronal injury level, flow cytometry demonstrated that GluN2B overexpression significantly alleviated LPS-induced apoptosis of HT22 cells, whereas BDNF knockdown suppressed this protective effect (Fig. 5F,G). Concurrently, LPS induced upregulation of the pro-apoptotic protein BAX, downregulation of the anti-apoptotic protein BCL-2, and decreased expression of PSD-95 and SYP in HT22 cells (Fig. 5H–J). GluN2B overexpression effectively reversed these aberrant protein expression changes and improved synaptic dysfunction; however, these protective effects were significantly counteracted by BDNF knockdown. In conclusion, GluN2B exerts a pivotal role in suppressing microglial M1 polarization, reducing neuronal apoptosis, and preserving synaptic function through regulation of the BDNF/TrkB signaling pathway. BDNF knockdown reverses most of the beneficial effects conferred by GluN2B overexpression, validating BDNF as an indispensable downstream molecule in this neuroprotective pathway.

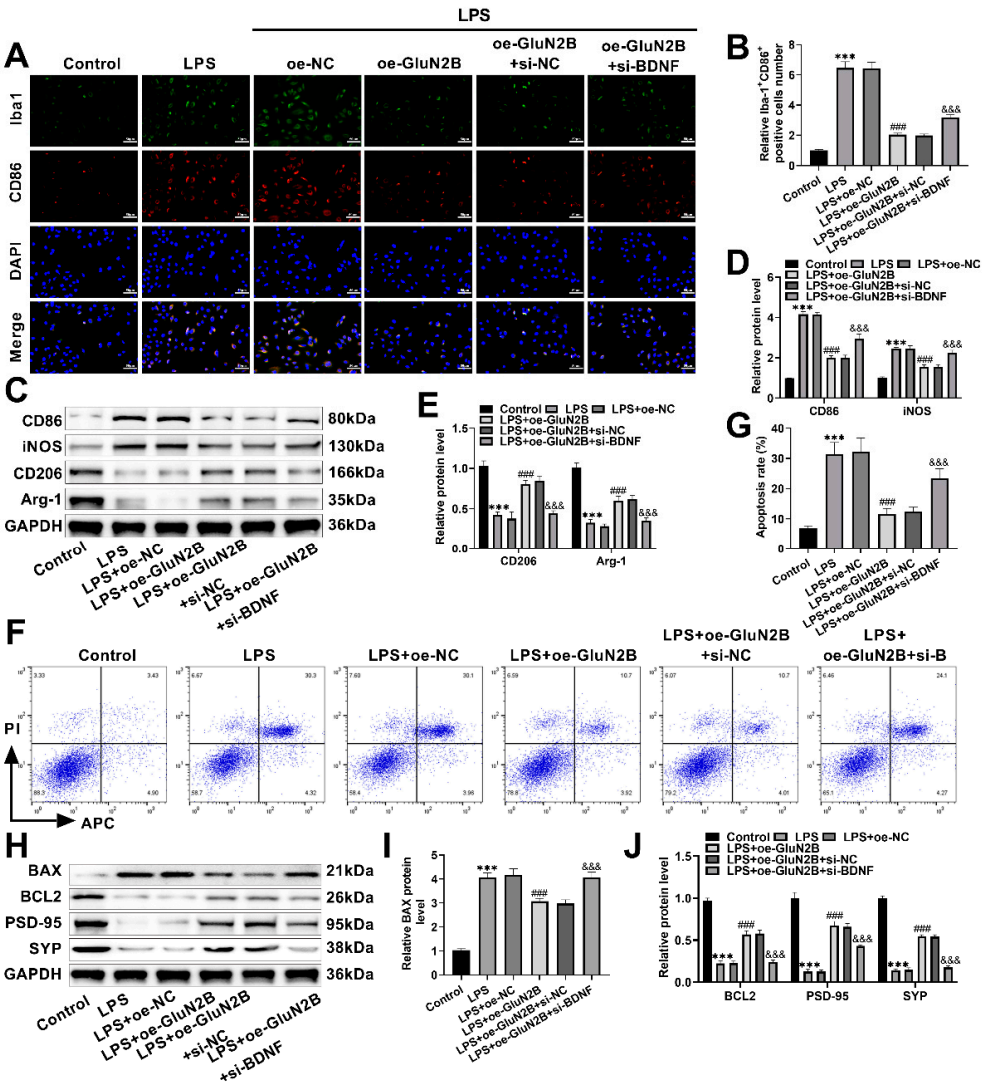

Figure 5: GluN2B regulation of BDNF/TrkB signaling improves LPS-induced neuroinflammation, neuronal injury, and synaptic dysfunction. (**A**,**B**) Immunofluorescence detection of co-expression of pro-inflammatory activation markers Iba1 and CD86 in microglia. Scale bar: 50 μm. (**C**–**E**) Analysis of CD86, iNOS, CD206, and Arg-1 expression in microglia. (**F**,**G**) Flow cytometry assessed apoptosis rates of HT22 neurons. (**H**–**J**) Western blot determination of BAX, BCL2, PSD-95, and SYP protein expression in HT22 cells. n = 6. $^{***}p < 0.001$ vs. Control; $^{\#\#\#}p < 0.001$ vs. LPS + oe-NC; $^{\&\&\&}p < 0.001$ vs. LPS + oe-GluN2B + si-NC.

3.6 Upregulation of GluN2B Ameliorates POCD in Aged Mice

To evaluate the therapeutic effect of GluN2B upregulation on POCD, a comprehensive analysis was conducted using behavioral tests and pathological assessments. Morris water maze results demonstrated that POCD model mice exhibited prolonged escape latency (Fig. 6A), with reduced time spent in the target quadrant and fewer crossings over the original platform location (Fig. 6B,C). Additionally, POCD mice showed impaired performance in fear conditioning tests (Fig. 6D), increased trial counts in the Y-maze (Fig. 6E), and decreased preference for novel objects in the NOR test (Fig. 6F), indicating deficits in learning and memory. Overexpression of GluN2B effectively reversed these behavioral impairments, significantly improving cognitive function.

TUNEL staining revealed a markedly increased percentage of apoptotic cells in the PFC of POCD mice, which was significantly reduced by GluN2B overexpression (Fig. 6G,H). HE staining showed that neurons in the prefrontal cortex of mice in the Sham group had intact structures, normal morphology, and were neatly arranged (Fig. 6I). In contrast, the POCD and POCD + oe-NC groups exhibited marked pathological damage, characterized by disorganized neuronal arrangement, loose cytoplasm, and pronounced nuclear pyknosis with deep staining. However, in the POCD + oe-GluN2B group, these histopathological lesions were substantially alleviated, and neuronal morphology tended toward normal. Nissl staining further confirmed that the Sham group displayed densely arranged, deeply stained Nissl bodies, indicative of high neuronal viability. In the POCD group, the number of neurons in the prefrontal cortex was markedly reduced, and the surviving neurons showed cytoplasmic atrophy and Nissl body condensation; overexpression of GluN2B significantly attenuated neuronal loss and the extent of neuronal damage (Fig. 6J,K). Collectively, in the aged mouse model of POCD, upregulation of GluN2B expression effectively ameliorated cognitive impairments such as deficits in learning and memory, reduced neuronal apoptosis and pathological injury in the prefrontal cortex, and exerted a neuroprotective effect.

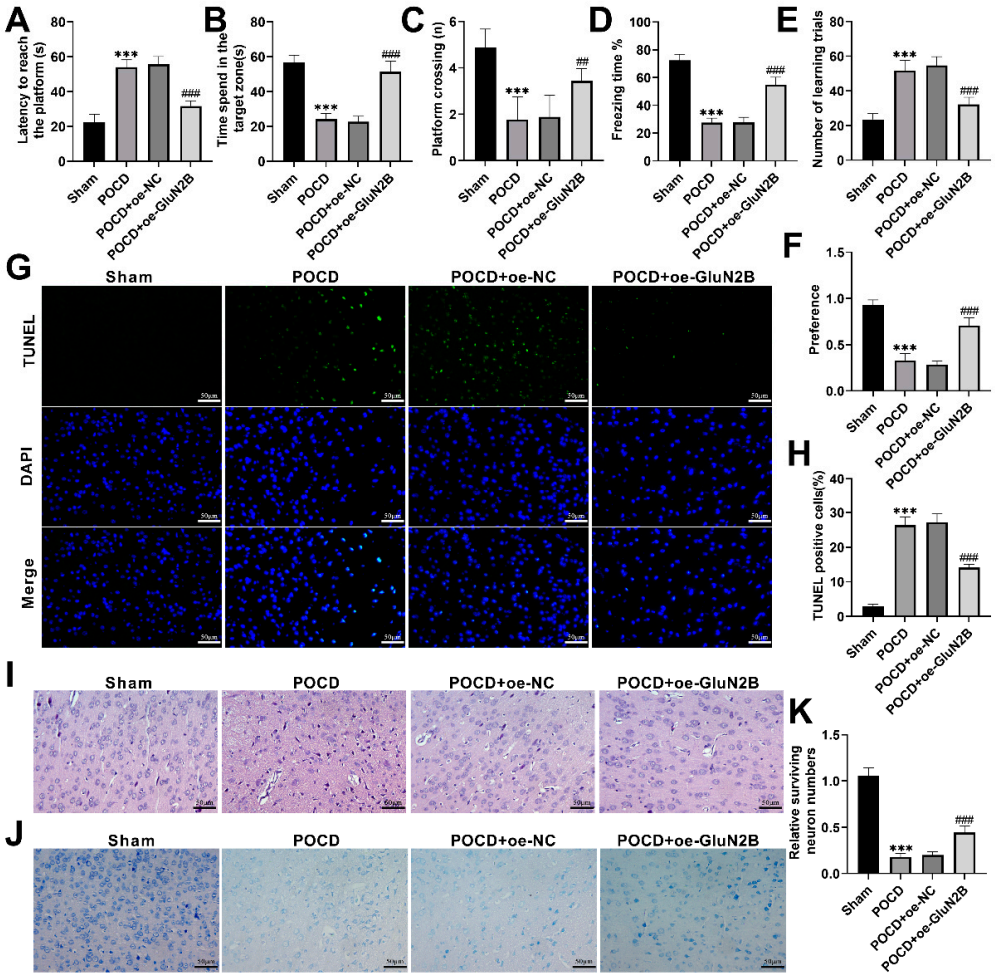

Figure 6: Upregulation of GluN2B improves POCD in aged mice. (**A**–**C**) Morris water maze test results evaluating animals' spatial learning and memory abilities, including escape latency, time spent in the target quadrant, and platform crossings. (**D**) Fear conditioning test to assess the mice memory and learning capacity. (**E**) The Y-maze test measures learning trial numbers to reflect spatial working memory. (**F**) NOR test evaluating recognition memory.

(**G**,**H**) TUNEL staining detects apoptotic cell proportions in the PFC of mice, reflecting neuronal apoptosis. Scale bar: 50 μm. (**I**) HE staining reveals histopathological changes in the PFC. Scale bar: 50 μm. (**J**,**K**) Nissl staining of brain sections assessing neuronal number and morphological alterations in the PFC. Scale bar: 50 μm. n = 9. $^{***}p < 0.001$ vs. Sham; $^{\#\#}p < 0.01$, $^{\#\#\#}p < 0.001$ vs. POCD + oe-NC.

3.7 GluN2B Targets the BDNF/TrkB Pathway to Ameliorate Neuroinflammation and Neural Injury

To elucidate the molecular mechanisms by which GluN2B improves POCD *in vivo*, key markers of the BDNF/TrkB pathway, neuroinflammation, and neuronal injury were assessed in the PFC. Western blot analysis showed that GluN2B, BDNF, and p-TrkB protein levels were significantly decreased in brain tissues from POCD model mice (Fig. 7A,B). GluN2B overexpression effectively reversed the downregulation of these proteins, markedly enhancing GluN2B, BDNF, and p-TrkB levels. Regarding neuroinflammation, immunofluorescence revealed a significant increase in Iba-1$^+$/CD86$^+$ (M1-type) microglia and a decrease in Iba-1$^+$/CD206$^+$ (M2-type) microglia in the PFC of POCD mice (Fig. 7C–F). ELISA assays further confirmed elevated pro-inflammatory cytokines, alongside decreased anti-inflammatory factors in POCD mice (Fig. 7G,H). Overexpression of GluN2B markedly reversed the aberrant microglial polarization and cytokine level.

In terms of neuronal injury and synaptic function, POCD mice showed increased expression of the pro-apoptotic protein BAX, decreased anti-apoptotic BCL-2, and significant reductions in the synaptic proteins PSD-95 and SYP (Fig. 7I–K). GluN2B overexpression significantly restored the expression of these proteins. These *in vivo* data indicate that upregulation of GluN2B ameliorates POCD by activating the BDNF/TrkB pathway, modulating microglial M2 polarization, attenuating neuroinflammatory responses, and ultimately inhibiting neuronal apoptosis and synaptic damage.

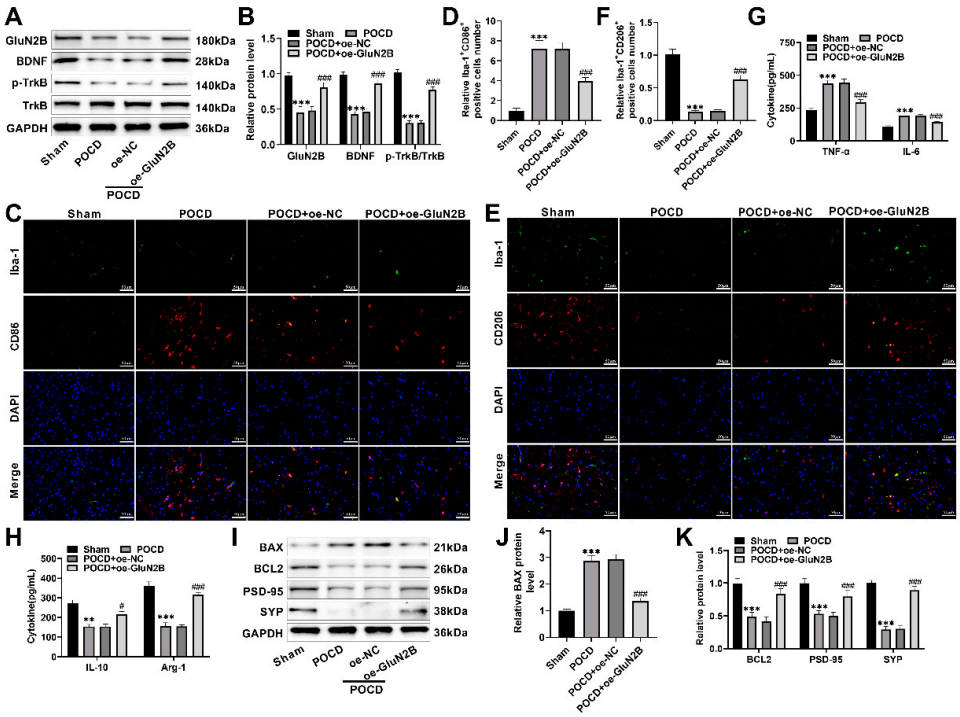

Figure 7: Upregulation of GluN2B targeting BDNF/TrkB signaling improves neuroinflammation and neuronal injury. (**A**,**B**) Western blot analysis of GluN2B, BDNF, p-TrkB, and TrkB protein levels in the PFC of mice. (**C**,**D**) Immunofluorescence analysis of co-expression of microglial markers Iba1 and CD86 in brain tissue. Scale bar: 50 μm.

(**E**,**F**) Immunofluorescence detection of co-expression of microglial markers Iba1 and CD206 in brain tissue. Scale bar: 50 μm. (**G**,**H**) ELISA detection of TNF-α, IL-6, IL-10, and Arg-1 levels in the PFC. (**I**–**K**) Western blot assessment of BAX, BCL2, PSD-95, and SYP protein expression in the brain. n = 9. $^{**}p < 0.01$, $^{***}p < 0.001$ vs. Sham; $^{\#}p < 0.05$, $^{\#\#\#}p < 0.001$ vs. POCD + oe-NC.

4 Discussion

POCD is a common neurological complication in elderly patients following anesthesia and surgery, with a complex pathogenesis involving neuroinflammation, synaptic dysfunction, and neuronal apoptosis [32,33]. This study systematically elucidated the critical role of GluN2B in regulating neuroinflammation and ameliorating POCD through both *in vivo* and *in vitro* experiments. In the LPS-induced microglial inflammation model, GluN2B expression was significantly downregulated, suggesting its involvement in the pathological process of neuroinflammation. As resident immune cells of the central nervous system, microglial polarization status is a key determinant of neuroinflammatory outcomes. M1-type microglia release large amounts of pro-inflammatory cytokines, contributing to neurotoxicity, whereas M2-type microglia secrete anti-inflammatory cytokines and neurotrophic factors, promoting tissue repair and neuroprotection [34,35]. Elevating GluN2B expression via gene overexpression significantly inhibited LPS-induced pro-inflammatory M1 polarization of microglia and promoted their polarization towards the anti-inflammatory M2 phenotype. This finding aligns with recent research trends regarding the roles of NMDAR subunits in immune cells [36].

This study further verified the indirect neuroprotective effect of GluN2B-mediated regulation of microglial activation on neurons using a co-culture system of microglia and HT22 neuronal cells. LPS-activated microglia significantly exacerbated HT22 neuron damage and apoptosis, accompanied by a marked reduction in the expression of synaptic markers SYP and PSD-95. SYP, a presynaptic vesicle protein, represents synaptic structural integrity, while PSD-95 is a key postsynaptic density scaffold protein; reductions in both directly reflect severe impairment of synaptic structure and function [37,38]. Pro-inflammatory cytokines, especially TNF-α and IL-6, have been shown to directly disrupt synaptic transmission and plasticity, for example, by promoting endocytosis of AMPA and NMDA receptors, thereby weakening synaptic strength [39,40]. In this study, GluN2B overexpression inhibited microglial M1 polarization and reduced pro-inflammatory cytokine release, attenuating inflammation-mediated synaptic toxicity. Moreover, a significant elevation of intracellular Ca^{2+} levels in neurons was observed, which is a critical inducer of excitotoxicity and apoptosis [41]. GluN2B overexpression restored Ca^{2+} homeostasis, suggesting its neuroprotective role may be associated with intracellular calcium signaling regulation. In summary, GluN2B attenuates microglia-mediated inflammatory insults, restores intracellular Ca^{2+} homeostasis in neurons, and maintains the expression of key synaptic proteins such as SYP and PSD-95, thereby providing multi-level, synergistic protection of synaptic structure and function. These findings offer more direct mechanistic evidence linking inflammation-induced synaptic damage to cognitive impairment in POCD.

Our study confirmed that GluN2B acts on the BDNF/TrkB signaling pathway to improve neuroinflammation and synaptic dysfunction. Experimental results clearly showed that LPS stimulation markedly suppressed BDNF expression and phosphorylation of its receptor TrkB, while GluN2B overexpression effectively reversed this suppression, significantly enhancing BDNF and p-TrkB levels. The BDNF/TrkB pathway is essential for neuronal survival, synaptic plasticity, and cognitive function maintenance [42,43]. BDNF activates TrkB receptors, initiating downstream signaling cascades such as MAPK and PI3K/Akt, promoting synaptogenesis, dendritic growth, and enhancement of synaptic

transmission, as well as upregulating synaptic proteins like SYP and PSD-95 [44]. Previous studies have widely recognized that POCD pathogenesis is closely associated with dysregulation of hippocampal BDNF/TrkB signaling. For instance, previous studies have reported that anesthesia- and surgery-induced NMDAR overactivation causes excessive calcium influx and activates the calcium-dependent protease calpain. Calpain then cleaves full-length TrkB, leading to BDNF/TrkB pathway dysfunction and subsequent cognitive impairment [45]. In our study, the activation of BDNF/TrkB signaling by GluN2B overexpression suggests neuroprotection may be achieved either by antagonizing downstream pathological events triggered by NMDAR overactivation (e.g., calpain-mediated TrkB cleavage) or by directly promoting BDNF expression and release [46].

To confirm the pivotal role of BDNF as an effector molecule in synaptic function within this pathway, rescue experiments were performed. Under GluN2B overexpression, BDNF knockdown significantly attenuated the inhibitory effect of GluN2B on microglial M1 polarization, its protective effect against neuronal apoptosis, and its improvement of synaptic protein expression. This provides strong evidence that the amelioration of neuroinflammation and synaptic dysfunction by GluN2B depends on activation of the BDNF/TrkB pathway. This finding aligns with recent studies highlighting the role of microglial-derived BDNF in regulating neuronal function [47,48]. BDNF released by M2-polarized microglia acts on neuronal TrkB receptors to not only directly promote neuronal survival but also importantly counteract inflammation-induced synaptic dysfunction through enhancing synaptic plasticity [21]. Our study confirms that upregulating GluN2B positively modulates the BDNF/TrkB signaling axis, thereby mediating microglial phenotypic switching and neuronal protection.

In vivo experiments, this study employed an aged mouse model of POCD and confirmed through behavioral tests that GluN2B overexpression significantly ameliorates cognitive impairments, including learning and memory deficits. Cognitive dysfunction is closely associated with impaired synaptic plasticity, consistent with the observed reduction of synaptic markers PSD-95 and SYP in the PFC in this study [49,50]. Molecular mechanism analysis aligned well with *in vitro* results: GluN2B, BDNF, and p-TrkB expression were downregulated in the PFC of POCD mice; the proportion of M1-type microglia increased, along with elevated levels of pro-inflammatory cytokines. GluN2B overexpression reversed all these pathological changes. These *in vivo* data not only validate the *in vitro* findings but also tightly link the GluN2B-BDNF/TrkB-neuroinflammation axis with POCD pathogenesis, suggesting its critical regulatory role in the onset and progression of cognitive impairment and its potential as a therapeutic target.

Although GluN2B, as a subunit of NMDARs, is mainly involved in regulating synaptic plasticity and excitatory transmission [51], this study emphasizes its key regulatory functions in non-neuronal cells (microglia) and neurotrophic factor signaling pathways. Future research could further explore how GluN2B regulates BDNF transcription or translation at the molecular level, as well as the precise localization and functions of GluN2B in microglia—for example, whether it influences the BDNF/TrkB pathway via non-channel functions such as scaffolding protein interactions. Moreover, given the side effects associated with clinical use of NMDAR inhibitors [52], targeting downstream effectors of GluN2B or developing strategies that selectively activate GluN2B-mediated BDNF/TrkB signaling may represent promising directions for translational research in POCD.

However, this study has certain limitations. First, we mainly employed a single LPS-induced inflammatory model and an aged mouse POCD model, which cannot fully capture the complex pathological processes of clinical POCD arising from multiple interacting factors, such as different anesthetic modalities, surgical types, and pre-existing comorbidities [53]. Second, GluN2B manipulation was primarily focused on the hippocampus and prefrontal cortex, and alterations in other cognition-related brain regions and

large-scale brain networks were not systematically evaluated. In addition, our mechanistic interpretation of GluN2B function mainly centers on the BDNF/TrkB pathway, while other downstream signaling cascades of GluN2B-containing NMDARs (such as ERK, JNK, or NF-κB) were not thoroughly explored [54]. Moreover, we have not yet validated the GluN2B–BDNF/TrkB–neuroinflammation axis in clinical patient samples, which to some extent limits the generalizability of our findings. These issues should be further addressed in future studies using multiple experimental models, additional brain regions, and translational clinical investigations.

5 Conclusion

This study demonstrates that GluN2B overexpression effectively inhibits microglial polarization toward the pro-inflammatory M1 phenotype by activating the BDNF/TrkB pathway. In turn, this mitigates neuroinflammation-mediated neuronal damage and synaptic dysfunction and ultimately improves POCD-related cognitive deficits in aged mice. This finding reveals a novel mechanism of GluN2B in the pathophysiology of POCD and provides an important theoretical basis for clinical interventions targeting the GluN2B-BDNF/TrkB signaling axis. However, the molecular mechanisms by which GluN2B regulates BDNF transcription or translation in microglia, as well as its precise localization and non-channel functions in microglia, remain to be fully elucidated. Future studies should focus on investigating the molecular role of GluN2B within microglia, particularly its regulation of BDNF gene transcription and protein translation.

Acknowledgement: None.

Funding Statement: This research was funded by the Shanghai Association of Chinese Integrative Medicine. (No. MT23-3) and Shanghai Municipal Health Commission. (No. 20224Y0201).

Author Contributions: [Bohan Lin]: Conceived and designed the research, conducted experiments, and analyzed data. Drafted and revised the manuscript critically for important intellectual content. [Wei Liu]: Contributed to the acquisition, analysis, and interpretation of data. Provided substantial intellectual input during the drafting and revision of the manuscript. [Xiu Ni, Fuyi Shen]: Participated in the conception and design of the study. Played a key role in data interpretation and manuscript preparation. All authors reviewed and approved the final version of the manuscript.

Availability of Data and Materials: The data that support the findings of this study are available from the corresponding author [Fuyi Shen], upon reasonable request.

Ethics Approval: All animal experiments in this study, including the isolation of primary microglial cells from neonatal mice and the grouped experiments conducted on aged mice, were performed under the same research project and approved by the Shanghai First Maternity and Infant Hospital, School of Medicine, Tongji University Ethics Committee (No. TJBG10522101).

Conflicts of Interest: The authors declare no conflicts of interest.

Abbreviations

Abbreviations	Full name
POCD	Postoperative Cognitive Dysfunction
BBB	Blood-Brain Barrier
NMDAR	N-Methyl-D-Aspartate Receptor
PFC	prefrontal cortex
BDNF	Brain-Derived Neurotrophic Factor
TrkB	Tropomyosin receptor kinase B
PKC	Protein Kinase C
Pyk2	Proline-rich Tyrosine Kinase 2

LDH	Lactate Dehydrogenase
NOR	Novel object recognition
SYP	Synaptophysin
TMEM119	Transmembrane Protein 119
P2RY12	Purinergic Receptor P2Y12

References

1. Bhushan S, Li Y, Huang X, Cheng H, Gao K, Xiao Z. Progress of research in postoperative cognitive dysfunction in cardiac surgery patients: A review article. Int J Surg. 2021;95:106163. [CrossRef].
2. Bertollo AG, Puntel CF, Albuquerque MFPA, Narzetti R, Ignácio ZM. The Impact of Lifestyle on Depression and Anxiety in Older Adults. Neurosci Res Clin Pract. 2025;1(1):1–15. [CrossRef].
3. Zhao Q, Wan H, Pan H, Xu Y. Postoperative cognitive dysfunction-current research progress. Front Behav Neurosci. 2024;18:1328790. [CrossRef].
4. Varpaei HA, Farhadi K, Mohammadi M, Khafaee Pour Khamseh A, Mokhtari T. Postoperative cognitive dysfunction: A concept analysis. Aging Clin Exp Res. 2024;36(1):133. [CrossRef].
5. Li Z, Zhu Y, Kang Y, Qin S, Chai J. Neuroinflammation as the underlying mechanism of postoperative cognitive dysfunction and therapeutic strategies. Front Cell Neurosci. 2022;16:843069. [CrossRef].
6. Tan XX, Qiu LL, Sun J. Research progress on the role of inflammatory mechanisms in the development of postoperative cognitive dysfunction. Biomed Res Int. 2021;2021:3883204. [CrossRef].
7. Li Y, Peng Q, Lu J, Hu L, Zhou H. Cognitive change associated with anesthesia and surgery: An introduction to POCD for neuroscientists. J Integr Neurosci. 2025;24(7):36785. [CrossRef].
8. Cheng C, Wan H, Cong P, Huang X, Wu T, He M, et al. Targeting neuroinflammation as a preventive and therapeutic approach for perioperative neurocognitive disorders. J Neuroinflamm. 2022;19(1):297. [CrossRef].
9. Wang C, Wang J, Zhu Z, Hu J, Lin Y. Spotlight on pro-inflammatory chemokines: Regulators of cellular communication in cognitive impairment. Front Immunol. 2024;15:1421076. [CrossRef].
10. Li N, Lu W, Tang L, Zhu L, Deng W, Liu H, et al. Microglia in post-traumatic brain injury (TBI) cognitive impairment: From pathological changes to therapeutic approaches. CNS Neurosci Ther. 2025;31(8):e70568. [CrossRef].
11. Pagano J, Giona F, Beretta S, Verpelli C, Sala C. N-methyl-d-aspartate receptor function in neuronal and synaptic development and signaling. Curr Opin Pharmacol. 2021;56:93–101. [CrossRef].
12. Zhang Y, Ren L, Min S, Lv F, Yu J. Effects of N-Methyl-D-aspartate receptor (NMDAR) and Ca^2+/calmodulin-dependent protein kinase IIα (CaMKIIα) on learning and memory impairment in depressed rats with different charge by modified electroconvulsive shock. Ann Transl Med. 2021;9(16):1320. [CrossRef].
13. Ge Y, Wang YT. GluN2B-containing NMDARs in the mammalian brain: Pharmacology, physiology, and pathology. Front Mol Neurosci. 2023;16:1190324. [CrossRef].
14. Chen QY, Li XH, Zhuo M. NMDA receptors and synaptic plasticity in the anterior cingulate cortex. Neuropharmacology. 2021;197:108749. [CrossRef].
15. Liu P, Wang C, Chen W, Kang Y, Liu W, Qiu Z, et al. Inhibition of GluN2B pathway is involved in the neuroprotective effect of silibinin on streptozotocin-induced Alzheimer's disease models. Phytomedicine. 2023;109:154594. [CrossRef].
16. Wang X, Xie J, Tan L, Lu Y, Shen N, Li J, et al. N6-methyladenosine-modified circRIMS2 mediates synaptic and memory impairments by activating GluN2B ubiquitination in Alzheimer's disease. Transl Neurodegener. 2023;12(1):53. [CrossRef].
17. Tian M, Stroebel D, Piot L, David M, Ye S, Paoletti P. GluN2A and GluN2B NMDA receptors use distinct allosteric routes. Nat Commun. 2021;12(1):4709. [CrossRef].
18. Li ZY, Liu Q, Shi XT, Jiao XH, Zhou Y, Chen C, et al. Impaired synaptic plasticity mediated by decreased GLUT1 in hippocampal astrocytes is involved in postoperative cognitive dysfunction in elderly mice. Mol Neurobiol. 2025;62(10):13678–96. [CrossRef].
19. Ali NH, Al-Kuraishy HM, Al-Gareeb AI, Alexiou A, Papadakis M, AlAseeri AA, et al. BDNF/TrkB activators in Parkinson's disease: A new therapeutic strategy. J Cell Mol Med. 2024;28(10):e18368. [CrossRef].

20. Li C, Sui C, Wang W, Yan J, Deng N, Du X, et al. Baicalin attenuates oxygen-glucose deprivation/reoxygenation-induced injury by modulating the BDNF-TrkB/PI3K/Akt and MAPK/Erk1/2 signaling axes in neuron-astrocyte cocultures. Front Pharmacol. 2021;12:599543. [CrossRef].
21. De Luca P, Mele M, Tanqueiro S, Napoli F, Butkevičiūtė U, Souto AC, et al. Synaptic accumulation of GluN2B-containing NMDA receptors mediates the effects of BDNF-TrkB signalling on synaptic plasticity and in hyperexcitability during status epilepticus. J Biomed Sci. 2025;32(1):82. [CrossRef].
22. Qiu LL, Pan W, Luo D, Zhang GF, Zhou ZQ, Sun XY, et al. Dysregulation of BDNF/TrkB signaling mediated by NMDAR/Ca^{2+}/calpain might contribute to postoperative cognitive dysfunction in aging mice. J Neuroinflamm. 2020;17(1):23. [CrossRef].
23. Wen Y, Xu J, Shen J, Tang Z, Li S, Zhang Q, et al. Esketamine prevents postoperative emotional and cognitive dysfunction by suppressing microglial M1 polarization and regulating the BDNF-TrkB pathway in ageing rats with preoperative sleep disturbance. Mol Neurobiol. 2024;61(8):5680–98. [CrossRef].
24. Shen Y, Zhang Y, Du J, Jiang B, Shan T, Li H, et al. CXCR5 down-regulation alleviates cognitive dysfunction in a mouse model of sepsis-associated encephalopathy: Potential role of microglial autophagy and the p38MAPK/NF-κB/STAT3 signaling pathway. J Neuroinflamm. 2021;18(1):246. [CrossRef].
25. Beeraka NM, Nagalakshmi A, Satyavathi A, Kote DM, Reddy YP, Basappa B, et al. Ginsenoside Rh4 Suppresses Notch3 and PI3K/Akt Pathway to Inhibit Growth and Metastasis of Gastric Cancer Cells: Ginsenoside Rh4 inhibit gastric cancer progression. J Can Biomol Therap. 2024;2(1):145–56. [CrossRef].
26. Zhao R, Zhao D, Zhu X, Li F, Xiong P, Li S, et al. The influence of miR-3149 on the malignancy progression of gastric cancer by negatively regulating CEACAM5. J Cancer Biomol Ther. 2024;1(1):1–10. [CrossRef].
27. Zhang M, Suo Z, Qu Y, Zheng Y, Xu W, Zhang B, et al. Construction and analysis of circular RNA-associated competing endogenous RNA network in the hippocampus of aged mice for the occurrence of postoperative cognitive dysfunction. Front Aging Neurosci. 2023;15:1098510. [CrossRef].
28. Xia P, Chen J, Liu Y, Cui X, Wang C, Zong S, et al. microRNA-22-3p ameliorates Alzheimer's disease by targeting SOX9 through the NF-κB signaling pathway in the hippocampus. J Neuroinflamm. 2022;19(1):180. [CrossRef].
29. Han X, Cheng X, Xu J, Liu Y, Zhou J, Jiang L, et al. Activation of TREM2 attenuates neuroinflammation via PI3K/Akt signaling pathway to improve postoperative cognitive dysfunction in mice. Neuropharmacology. 2022;219:109231. [CrossRef].
30. Kim Y, Hwang I, Kim S, Jeung EB. Effects of TBBPA exposure on neurodevelopment and behavior in mice. Int J Mol Sci. 2025;26(15):7289. [CrossRef].
31. Kenkhuis B, Somarakis A, Kleindouwel LRT, van Roon-Mom WMC, Höllt T, van der Weerd L. Co-expression patterns of microglia markers Iba1, TMEM119 and P2RY12 in Alzheimer's disease. Neurobiol Dis. 2022;167:105684. [CrossRef].
32. Zhang M, Yin Y. Dual roles of anesthetics in postoperative cognitive dysfunction: Regulation of microglial activation through inflammatory signaling pathways. Front Immunol. 2023;14:1102312. [CrossRef].
33. Zhang Y. Changes of neuronal plasticity in postoperative cognitive dysfunction (POCD). Alzheimers Dement. 2021;17(S2):e058460. [CrossRef].
34. Peng W, Lu W, Jiang X, Xiong C, Chai H, Cai L, et al. Current progress on neuroinflammation-mediated postoperative cognitive dysfunction: An update. Curr Mol Med. 2023;23(10):1077–86. [CrossRef].
35. Tang CC, Liu DX, Zhu ZQ. Research progress of microglial surface receptors in perioperative neurocognitive disorders. Ibrain. 2024;10(4):450–61. [CrossRef].
36. Guan S, Li Y, Xin Y, Wang D, Lu P, Han F, et al. Deciphering the dual role of N-methyl-D-Aspartate receptor in postoperative cognitive dysfunction: A comprehensive review. Eur J Pharmacol. 2024;971:176520. [CrossRef].
37. Haseena PA, Basavaraju N, Chandran M, Jaleel A, Bennett DA, Kommaddi RP. Mitigation of synaptic and memory impairments via F-actin stabilization in Alzheimer's disease. Alzheimers Res Ther. 2024;16(1):200. [CrossRef].
38. Leung E, Lau EW, Liang A, de Dios C, Suchting R, Östlundh L, et al. Alterations in brain synaptic proteins and mRNAs in mood disorders: A systematic review and meta-analysis of postmortem brain studies. Mol Psychiatry. 2022;27(3):1362–72. [CrossRef].
39. Zhang J, Zheng X, Zhang G, Cheng Z, Liu Y, Zhang L, et al. Chronic postoperative pain induces contextual fear extinction dysfunction through hippocampal NMDAR/BDNF/TrkB signaling pathway in mice. Transl Psychiatry. 2025;15(1):203. [CrossRef].

40. Benarroch E. What is the role of cytokines in synaptic transmission? Neurology. 2024;103(8):e209928. [CrossRef].
41. Sukumaran P, Nascimento Da Conceicao V, Sun Y, Ahamad N, Saraiva LR, Selvaraj S, et al. Calcium signaling regulates autophagy and apoptosis. Cells. 2021;10(8):2125. [CrossRef].
42. Wang F, Li Y, Tang D, Yang B, Tian T, Tian M, et al. Exploration of the SIRT1-mediated BDNF-TrkB signaling pathway in the mechanism of brain damage and learning and memory effects of fluorosis. Front Public Health. 2023;11:1247294. [CrossRef].
43. Soman SK, Swain M, Dagda RK. BDNF-TrkB signaling in mitochondria: Implications for neurodegenerative diseases. Mol Neurobiol. 2025;62(2):1756–69. [CrossRef].
44. Barde YA. The physiopathology of brain-derived neurotrophic factor. Physiol Rev. 2025;105(4):2073–140. [CrossRef].
45. Mao L, Wang L, Huang Z, Switzer JA, Hess DC, Zhang Q. Perioperative neurocognitive disorders: Advances in molecular mechanisms and bioactive molecules. Ageing Res Rev. 2025;112:102885. [CrossRef].
46. Chen R, Chen W, Li P, Zhao Y, Zeng Q, Chen W, et al. Function and application of brain-derived neurotrophic factor precursors (Review). Int J Mol Med. 2025;56(1):1–20. [CrossRef].
47. Komori T, Okamura K, Ikehara M, Yamamuro K, Endo N, Okumura K, et al. Brain-derived neurotrophic factor from microglia regulates neuronal development in the medial prefrontal cortex and its associated social behavior. Mol Psychiatry. 2024;29(5):1338–49. [CrossRef].
48. Tang R, Cao QQ, Hu SW, He LJ, Du PF, Chen G, et al. Sulforaphane activates anti-inflammatory microglia, modulating stress resilience associated with BDNF transcription. Acta Pharmacol Sin. 2022;43(4):829–39. [CrossRef].
49. Ribarič S. Detecting early cognitive decline in Alzheimer's disease with brain synaptic structural and functional evaluation. Biomedicines. 2023;11(2):355. [CrossRef].
50. Si J, Chen X, Qi K, Li D, Liu B, Zheng Y, et al. Shengmaisan combined with Liuwei Dihuang Decoction alleviates chronic intermittent hypoxia-induced cognitive impairment by activating the EPO/EPOR/JAK2 signaling pathway. Chin J Nat Med. 2024;22(5):426–40. [CrossRef].
51. Tahiri E, Corti E, Duarte CB. Regulation of synaptic NMDA receptor activity by post-translational modifications. Neurochem Res. 2025;50(2):110. [CrossRef].
52. Egunlusi AO, Joubert J. NMDA receptor antagonists: Emerging insights into molecular mechanisms and clinical applications in neurological disorders. Pharmaceuticals. 2024;17(5):639. [CrossRef].
53. Arefayne NR, Berhe YW, van Zundert AA. Incidence and factors related to prolonged postoperative cognitive decline (POCD) in elderly patients following surgery and anaesthesia: A systematic review. J Multidiscip Healthc. 2023;16:3405–13. [CrossRef].
54. Mitrović N, Adžić Bukvić M, Zarić Kontić M, Dragić M, Petrović S, Paunović M, et al. Flaxseed oil alleviates trimethyltin-induced cell injury and inhibits the pro-inflammatory activation of astrocytes in the hippocampus of female rats. Cells. 2024;13(14):1184. [CrossRef].